Enhancement of photoconversion efficiency and light harvesting ability of TiO_2 nanotube-arrays with Cu_2ZnSnS_4

Athil Al-Shihabi Al-Ani [a], Begum Tokay [a,*], Wen Zhu [b,*], George Z. Chen [a,*]

a: Advanced Material Research Group, Faculty of Engineering, University of Nottingham, Nottingham NG7 2RD, UK

b: School of Material Science and Engineering, Department of Material Science and Technology, Huazhong University of Science & Technology, Wuhan 430074, P. R. China

* Corresponding authors: begum.tokay@nottingham.ac.uk; george.chen@nottingham.ac.uk; wennar@mail.hust.edu.cn

Abstract

We report an underpotential deposition (UPD) route of Cu_2ZnSnS_4/TiO_2 nanotube arrays (TiO_2-NTAs) in which the Kesterite (Cu_2ZnSnS_4) was employed as a sensitizer to enhance the photoconversion efficiency of the TiO_2-NTAs. Cu_2ZnSnS_4 was simultaneously coated on TiO_2-NTAs by depositing its constituent metals from the precursor ions *via* electrochemical atomic layer deposition (EC-ALD) and subsequent annealing. The detailed synthesis process, the surface morphology, crystalline structure, photoelectrochemical properties and hydrogen production rate of the as-prepared Cu_2ZnSnS_4/TiO_2-NTAs were discussed. Thickened TiO_2 nanotubes were observed, suggesting that the Cu_2ZnSnS_4 coating was about 5 ± 0.5 nm. The results showed that the light harvesting of TiO_2-NTAs has an obvious improvement after sensitizing them with Cu_2ZnSnS_4. In comparison with pure TiO_2-NTAs, a two-fold increment in photoconversion efficiency was achieved using the composite of Cu_2ZnSnS_4/TiO_2-NTAs. The novel photoanode of CZTS/TiO_2 NTAs achieved a maximum hydrogen generation rate of 49 ml h^{-1} cm^{-2}.

Keywords: CZTS; EC-ALD, photoconversion efficiency; TiO_2 nanotube arrays (NTAs); Underpotential deposition

1. Introduction

Environmental pollution and energy crisis are currently two major problems that have enormously hindered and threatened the development of human civilization. The photocatalytic technologies could be considered as an effective pathway to resolve these problems since they can provide clean hydrogen energy *via* splitting the water by irradiating a photoanode with solar energy. The key reactions in the photocatalysis are water reduction and oxidation, which have been extensively studied, since the pioneering work by Honda and Fujishima in 1972 [1, 2]. Based on this discovery, studies focused on finding the most suitable semiconductor, which assists the photo splitting of water [3, 4]. So far, a large number of heterogeneous semiconductors (SCs) have been studied in water splitting (WS), due to their ability to driven the visible-light such as CoO, Ag_3PO_4, $BiVO_4$, Ta_3N_5, TaON, C_3N_4 [2], WO_3 and Fe_2O_3 [5]. However, most of these SCs have revealed a low efficiency in the practice.

In the last three decades, the vertically oriented TiO_2 nanotube arrays (NTAs), which synthesized on a titanium (Ti) foil *via* the electrochemical anodization route, have been studied among all of the TiO_2 nanostructured materials and exceedingly become in demand [6, 7]. Several studies [5, 8, 9] reported that the NTAs have shown superior electron lifetimes and high photocurrent densities in comparison to the nanoparticles. Zhu et al. reported a maximum H_2 generation rate (10.24 ml h^{-1} cm^{-2}) from CdSe (6 h)/CdS (4 cycles)/ TiO_2 NTs photoelectrode [10]. These highly ordered NTAs have also had unique electrical properties, which can meet all requirements of photoelectrolysis, such as suitable band gap with matching the energy band for H_2 and O_2 evolution and good stability in the electrolyte against the photocorrosion [2, 11, 12]. Besides, the well-suited large specific surface areas of the NTAs plays a vital role in their uniqueness. They serve the availability of a large number of active reaction sites for the chemical reactions, and many ions in the solution can get access to the photogenerated holes [13-16]. However, the anatase phase of TiO_2 has a large band gap (3.2 eV), which limits its activation only in the UV region (4-5% of solar energy spectrum). It has been reported that the wide band gap of TiO_2 can be coupled with a narrow band gap semiconductor (sensitizer) to form a heterogeneous structure, which in turn can enhance the charge separation and visible light harvest [17].

The Cu_2ZnSnS_4 (CZTS) is recently considered as a promising and efficient candidate for the absorber of the thin film type solar cells [18] due to its narrow band gap (1.4-1.5 eV) and large optical absorption coefficient (~104 cm^{-1}) [19]. It is an environmentally friendly semiconductor, and its constituents are cheap and earth abundantly [20]. Various approaches have been used to synthesise the thin film CZTS including chemical methods such as photochemical deposition and sol-gel spin-coated deposition and physical vapour methods e.g. co-evaporation and hybrid sputtering. Previous studies demonstrated that it is

challenging to prepare the thin film CZTS with a controlled stoichiometry and high conversion efficiency (theoretical efficiency > 30%) [21] by using common synthetic methods. Wang et al.have synthesised the thin film CZTS using a spin coating method with the highest efficiency of 12.6% [22]. Nguyen et al. studied the effect of annealing on the crystallisation of the CZTS absorber, which was prepared by the hot-injection method and reported a conversion efficiency of 4.94% [23]. Wang and Demopoulos have studied the growth of CZTS nanocrystalline on TiO_2 nanorod arrays *via* the controlled method successive-ion-layer-adsorption-reaction (SILAR) [24]. Although they have achieved an internal quantum efficiency of ~ 60% with a short circuit current density of 3.22 $mA.cm^{-2}$, they required to heat the reaction solution. Lin et al. (2016b) fabricated the quaternary CZTS using the sputtering route [25]. They obtained an approximate stoichiometry of 2:1:1:4 of CZTS but with uncontrollable film thickness. Recently, Gan et al. synthesised CZTS on TiO_2 nanosheet arrays via a two-step hydrothermal method over 24 h period and reported a degradation rate for methyl orange that is 6.6 times higher than that of the pure TiO_2 nanosheet arrays [26]. Alternatively, Wang et al. showed an electrochemical deposition route of nano Al_2O_3 layer on CZTS-TiO_2 nanorods to improve band alignment. Spin coating method was employed to deposit CZTS on the TiO_2 nanorods. After further coating and modifications, the energy conversion efficiency of the solar cell fabricated was improved by 4.2% [27]. Alternatively, Bugato et al. utilised robotic spray pyrolysis deposition to obtain an active photocatalyst thin film with the CZTS/TiO_2 heterostructure on glass substrate [28]. They studied the long-term stability and photocatalytic activity (up to 72 h) of the Cu_2ZnSnS_4/ TiO_2 thin film heterostructures, under simulated solar radiation. Although, they reported high removal efficiencies for phenol (73%) and imidacloprid (57%) photocatalyst was not stable after 48 h due to degradation.

Although a variety of methodologies have been reported to integrate the TiO_2 NTAs with sensitizers, most of these methods easily lead to plug the pore mouth of the nanotubes by the precipitation of the sensitizer, and thus reduce the adsorption capacity and the specific surface area. The EC-ALD is considered as one of the most efficient methods, compared to the other techniques, meeting the requirements for preparing heterojunctions [10]. Commercially, EC-ALD consumes relatively small amount of energy and can be performed under ambient conditions. The deposition in low temperature has the benefit of avoiding the heat-induced interdiffusion of component elements and interfacial structure degradation. Moreover, the vacuum atmosphere is not necessary [29, 30]. Ghosh et al were the first to show that EC-ALD is capable of controlling a precise thickness by angstrom resolution and coverage of high aspect ratio nanostructures; thus, the targeted thickness of the desired compound is controlled by the number of EC-ALD cycles of the precursor

molecules (metal ions), which in turn ensure a self-limiting of substrate surface reactions [31].

The photoelectric conversion and H_2 evolution of TiO_2 nanotube arrays have been widely reported [32-36]. Cao et al. deposited Bi/Bi_2MoO_6 nanoparticles on TiO_2 NTAs by a solvothermal method and reported the hydrogen production rate as 73.41 μmol h^{-1} cm^{-2} [32]. Similarly, Jia et al. utilised solvothermal method to synthesise Bi_2S_3-BiOBr on TiO_2 NTA and Ti mesh and achieved hydrogen generation amount of 60.41 μmol cm^{-2} after 3.5 h visible light irradiation [33]. Li et al. designed a new photoelectrochemical cell based on membrane electrode assembly on TiO_2/Ti mesh and measured the hydrogen evolution rate of 0.57 ml h^{-1} cm^{-2} [37]. Li et al. reported the hydrogen 24.83 mmol g^{-1} h^{-1} for their TiO_2 catalyst due to doping with Cu_2O [38]. Fan et al. successfully increased the hydrogen evolution rate to 1.35 μmol h^{-1} cm^{-2} of pure TiO_2 NTAs from 0.47 μmol h^{-1} cm^{-2} after doping with Ag and Fe [39].

To obtain an excellent optical absorption and enhance photoconversion efficiency of TiO_2 NTAs, researchers have also studied the electrodeposition of the thin film CZTS on various substrates, such as TiO_2 nanorods (NRs) [40], Ag [41] and indium tin oxides (ITO) [42]. Ho and Chen [43] have employed the nanocrystal CZTS to decorate the surface of TiO_2 NRs to induce its conversion efficiency and improve the hydrogen generation rate. They demonstrated that the current density increased from 2.92 mA cm^{-2} to 6.91 mA cm^{-2} and the conversion efficiency increased from 1.44% to 3.50%. However, the TiO_2 NRs are offered relatively small light absorption areas in comparison with the highly ordered TiO_2 NTAs [44, 45].

Although various methodologies have been employed to investigate the electrodeposition of several types of semiconductors (binary or ternary) onto TiO_2 NTAs, most of them have missed highlighting the simultaneous electrodeposition of the quaternary CZTS *via* the underpotential deposition route. In this study, for the first time, we successfully illustrated the one-step EC-ALD of the quaternary compound CZTS onto TiO_2 NTAs electrodes to simultaneously form coaxial heterogeneous structure. We determined the underpotential deposition potentials of the multiple elements by using cyclic voltammetry (CV). Detailed structural, morphology and quantitative characterization was performed using X-ray diffraction (XRD), Field Emission Gun-Scanning Electron Microscopy (FEG-SEM) and Energy-Dispersive X-ray spectroscopy (EDX), respectively. The photoelectrochemical properties and hydrogen production rate of the resulting coaxial heterogeneous structure CZTS TiO_2 NTAs were provided in this study.

2. Experimental

2.1 Preparation of TiO_2 NTAs

The TiO_2 NTAs were successfully synthesised *via* an electrochemical anodization technique using Agilent DC power supply (6645A, 0.0 to 120.0 V / 0.0 to 1.5 A). Prior to anodization, a Ti foil (Unicorn Metals Ltd., thickness 0.2 mm and purity 99.9%) was cut into 35 mm × 10 mm, then cleaned with acetone and deionized water for 30 min in an ultrasonic bath, respectively then dried under nitrogen flow. The anodization electrolyte contained 0.32 wt% ammonium fluoride (NH_4F, Sigma Aldrich, ≥98%), which was added to 40 ml ethylene glycol ($C_2H_6O_2$, Fisher, Laboratory reagent grade) in a glass jar container and 4 vol% of high purity water (resistivity=0.0476 MΩ-cm) was slowly added to the ethylene glycol for 1 h with constant stirring. The anodization cell was formed of two electrode configurations, a Ti sheet as an anode (WE) and a Pt wire (CH Instrument, 1 mm diameter) as a cathode (CE).

The anodization was performed in two steps: 1. 2 min anodization at a constant bias applied voltage of 60 V. The sample was washed with plenty of high purity water and soaked into ethanol (Sigma Aldrich, ≥99.8%) for 5 min to completely remove the residual electrolyte and left to dry naturally in air; this was followed by thermal annealing at 700 ℃ for 1 h (at a heating and cooling rate of 2 ℃ min^{-1}) in tube furnace (Elite TSH 12/50/300-2416). 2. 6 h anodization at a constant bias applied voltage of 60 V; then the sample was soaked in ethanol for 10 min and annealed at 450 ℃ for 2 h (at a heating and cooling rate of 2 ℃ min^{-1}) to convert the amorphous phase to an anatase crystalline phase.

2.2 Deposition of Cu_2ZnSnS_4 onto TiO_2 NTAs *via* EC-ALD

Aqueous electrolytes of Cu, Zn and Sn were prepared separately by mixing 0.02 M $CuSO_4$ (Sigma Aldrich, purity ≥ 99%), 0.20 M $ZnSO_4$ (Sigma Aldrich, ≥ 99%) and 0.01 M $SnCl_2$ (Sigma Aldrich, ≥ 98%) in deionised water. Sn solution was further centrifuged (20,000 rpm, 30 min) to obtain a well-dissolved solution to eliminate the excess of tin hydroxide ($Sn(OH)_2$), which was suspended in the water due to impurities present in the powder ($SnCl_2$). 0.2 M of trisodium citrate dihydrate ($Na_3C_6H_5O_7$, Sigma Aldrich, ≥ 98%) was added to each electrolyte.

Degassing step was performed by purging N_2 into the precursor solutions for 30.0 m to remove the dissolved oxygen. The air exposure to the precursor solutions was minimised by sealing the containers using Parafilm. The electrolytes were mixed on magnetic stirrers for 2.0 h. The pH value of the solutions was adjusted by 5 M NaOH and 0.5 M acetic acid solutions to reach 6.5.

The UPD potential range for the for the simultaneous deposition of each element determined using CV measurements. The UPD indicates to the onset electrochemical deposition of metal atoms onto a foreign substrate because the metal-substrate bond strength is greater than the metal-metal bond strength. Therefore, deposition begins at potential ranges

more positive than the equilibrium potential (described by Nernst equation) for the reduction of this metal, thus, the resulting deposit is generally limited to less than a monolayer. The UPD shift refers to the difference between the potential oxidation peak for a layer of a metal adsorbed on a foreign substrate and the potential of the corresponding reduction peak of the pure metal. The UPD potentials of the multielements essentially should lie in a common region, so the resulting deposited film will generally be limited to an atomic layer. The UPD potential is measured *via* cyclic voltammetry, which involves monitoring the current continuously within the linear scanning for the potential of the working electrode at a constant scan rate between two selected limits (start and end potentials). Due to the double layer charging, any reaction at the electrode can be detected as an overlaid current. The UPD potential of the metal adsorbate is represented by two cathodic (deposition) and anodic (dissolution) current density peaks.

After determining the UPD potential range for the simultaneous deposition of each element and adjusting the pH of the individual precursor solutions, the precursor solutions were mixed on a magnetic stirrer for 15 min, and the final pH of the electrodeposition bath was recorded. Ethylenediaminetetraacetic acid (0.1 and 0.3 M $EDTA^{2-}$, Fisher, 99%) was used as a complexing agent to shift the UPD potential towards the negative side, where needed. Subsequently, the electrodeposition was carried out for 7 h at room temperature by employing an electrochemical workstation (Metrohm, PGSTAT100 Autolab Co., Ltd, UK). The electrode configuration is shown in Figure 1.

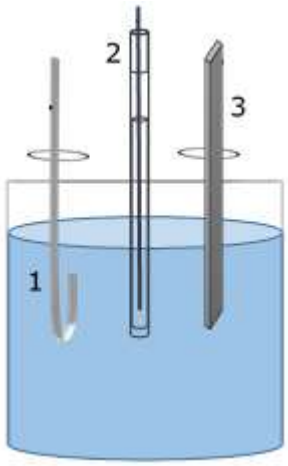

Figure 1. Configuration of electrodes for electrochemical deposition 1) Platinum wire Pt (CE), (2) reference electrode Ag/AgCl (RE) and (3) TiO_2 NTA working electrode (WE).

After electrodeposition of Cu, Zn and Sn, the coated sample was rinsed with deionised water (DIW) and left to dry naturally for 16 h and transferred to a tube furnace (Elite, TSH 12/50/300-2416) for annealing step at 585 ℃ for 2 h in nitrogen flowrate of 20 ml min^{-1}. The nitrogen function was to carry the sulfur vapour inside the tube and to remove any impurities

or by-products that may be produced during the sulfurization. Two ceramic boats were placed inside the quartz tube in the furnace: the first one contains elemental sulfur (2 g, Sigma Aldrich, 99.50-100.50%), followed by another one where the coated substrate was placed.

The CV experiments were performed within the following applied potential ranges for Cu (-1.5 to 1.0 V), Zn (-0.35 to 0.85 V) and Sn (-0.5 to 1.5 V). Measurements were carried out at the scan rate = 20 mV s^{-1}.

2.3 Determination of photoelectrocatalytic properties

The images of the samples (CZTS/TiO_2 NTAs) were observed by field-emission scanning electron microscopy (7100F FEG-SEM, JEOL). The crystalline phase was verified using an X-ray diffractometer (D8 Advance, Bruker). The photocatalytic performance of the novel CZTS/TiO_2 NTAs composite was examined in a photoelectrochemical cell (PEC) with Pt wire as a counter electrode and the resulting CZTS/TiO_2 NTAs as working electrode. The measurements were conducted in an electrolyte containing 0.28 M of sodium sulfide (Na_2S) and 0.32 M of sodium sulfite (Na_2SO_3) as sacrificial reagents under illumination (100 mW cm^{-2}) using a light source (500 W Xe DC Mercury Xenon arc lamps, Newport). This light source was connected to a power supply, and the illumination was performed using a current of 7.7 A.

The photocurrent density of TiO_2 NTAs before and after the deposition was measured. The TiO_2 NTAs substrate (35 mm × 10 mm) was exposed to the light source placed at 5 cm distance, and it was biased by applying a voltage of open circuit potential 1.5 V. The current was simultaneously recorded. The photoconversion efficiency of TiO_2 NTAs and CZTS/TiO_2 NTAs was calculated using the following formula:

$$\eta(\%) = j_p \left[\frac{E^0_{Rev} - |E_{app}|}{I_0}\right] 100 \quad [1]$$

where E^0_{Rev} (total power output), which is the potential (= 1.23 V) corresponding to the Gibbs Free Energy change per photon in the water-splitting reaction. E_{app} (electric power input) = E_{meas} - E_{aoc}, wherein E_{meas} is the electrode potential vs. Ag/AgCl of the working electrode, and E_{aoc} is the electrode potential vs. Ag/AgCl of the same working electrode at open-circuit condition under the same illumination and in the same electrolyte. j_p is the corresponding photocurrent density, and I_0 (light power input) denotes the intensity of incident light [46]. The bandgap energy (Eg) was calculated from the relationship between the absorbance ($\propto$) and the incident photon energy ($h\nu$) shown in Equations 2 and 3 by applying Tauc relation [47], respectively:

$$h\nu = 1240/\lambda \quad [2]$$

$$\propto h\nu = A\,(h\nu - Eg)^{m} \qquad [3]$$

where A is a constant dependent on the transition probability, and m is equal to 0.5 for the indirect gap and 2.0 for the direct gap. The bandgap energy was calculated from the plot of $(\propto h\nu)^{1/2}$ vs. incident photon energy $(h\nu)$ [47, 48] by extrapolating to zero using a linear fit [49].

The hydrogen generation rate was measured for 30 min by employing Hoffman Voltameter (Scientific Glass Laboratories) under light irradiation, using the same light source and sacrificial agents. The experiment was performed at the applied potential of -0.5 V. H_2 production was observed at the cathode and recorded every 10 min.

3 Results and Discussions

3.1 UPD determination

Figure 2 shows the CV measurements of Cu, Zn and Sn on separate TiO_2 NTAs substrates. The UPD of each element was determined from individual solutions by applying different potential ranges. Figures 2a and b depict series of voltammograms, which performed until the UPD and bulk potentials of Cu and Sn were observed. It is essential to find out the bulk deposition potential of a metal to avoid the accumulation of its ions on the substrate, which may cause clogging the tube pore mouth, and consequently weaken the TiO_2 NTAs light absorption.

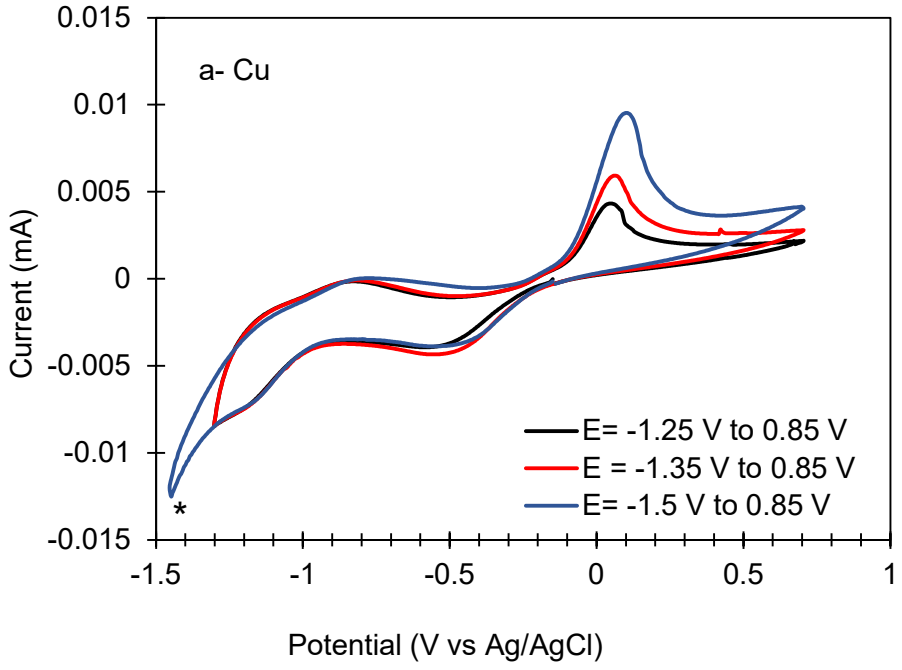

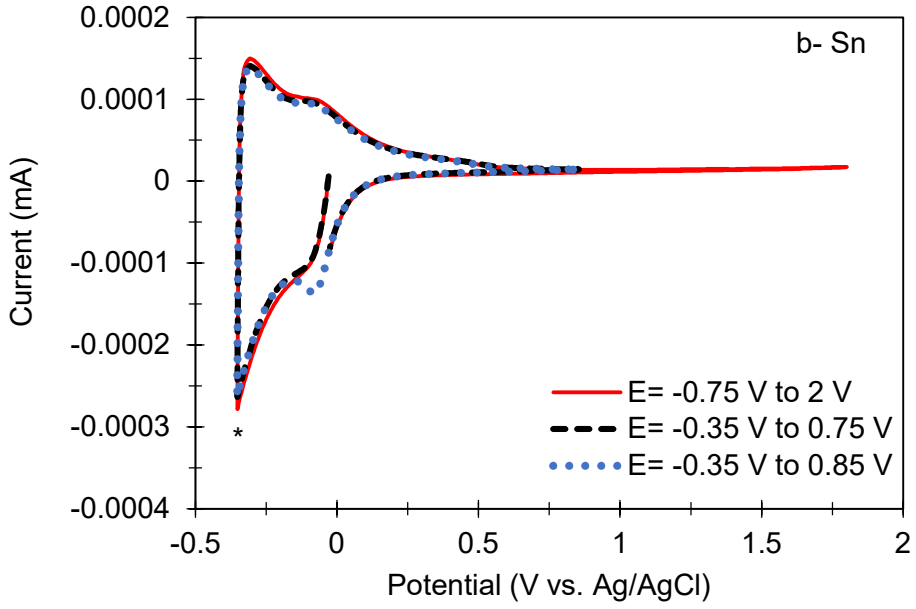
b- Sn
Current (mA)
Potential (V vs. Ag/AgCl)
E= -0.75 V to 2 V
E= -0.35 V to 0.75 V
E= -0.35 V to 0.85 V
*
0.0002
0.0001
0
-0.0001
-0.0002
-0.0003
-0.0004
-0.5
0
0.5
1
1.5
2

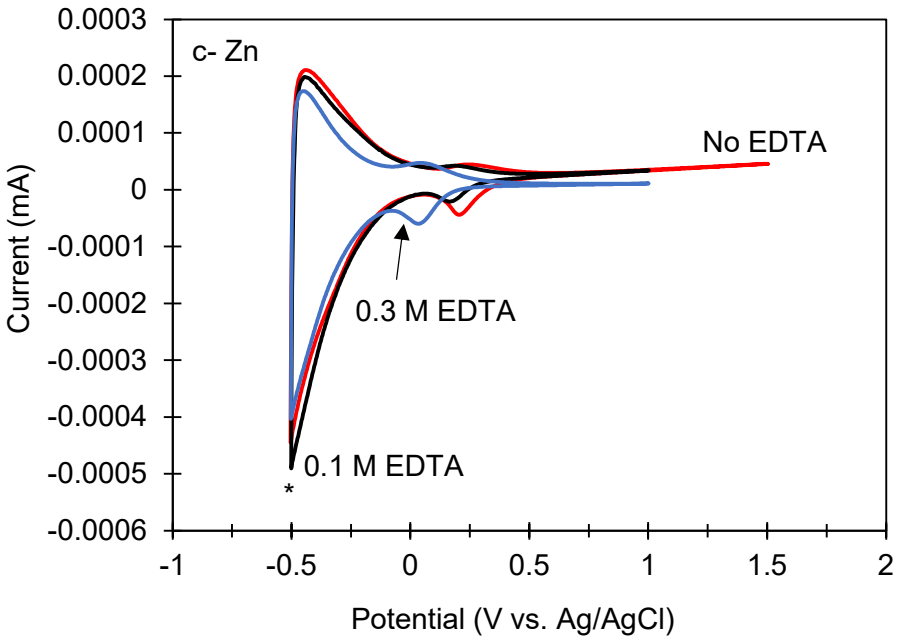
c- Zn
Current (mA)
Potential (V vs. Ag/AgCl)
No EDTA
0.3 M EDTA
0.1 M EDTA
*
0.0003
0.0002
0.0001
0
-0.0001
-0.0002
-0.0003
-0.0004
-0.0005
-0.0006
-1
-0.5
0
0.5
1
1.5
2

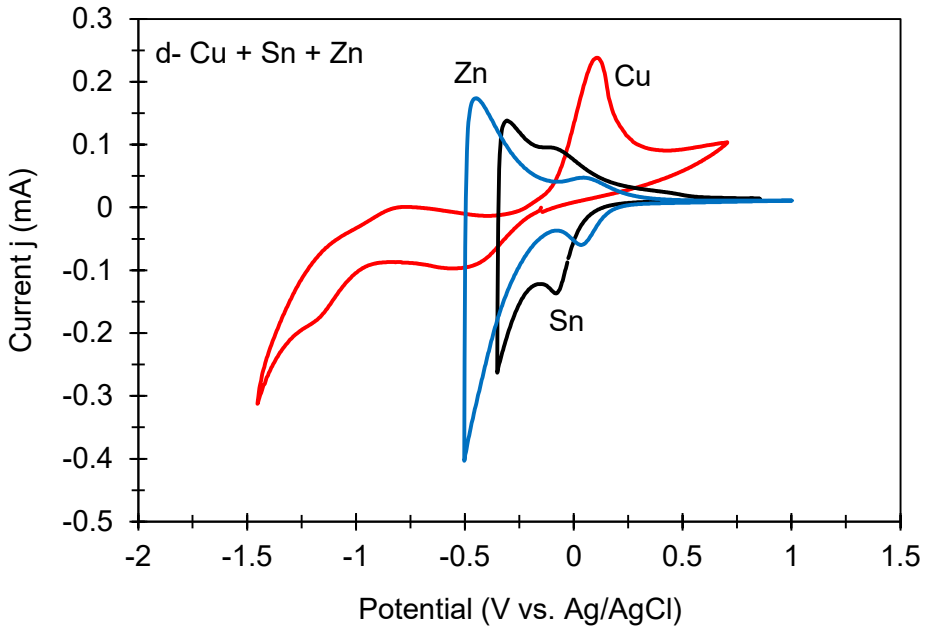
d- Cu + Sn + Zn
Current j (mA)
Potential (V vs. Ag/AgCl)
Zn
Cu
Sn
0.3
0.2
0.1
0
-0.1
-0.2
-0.3
-0.4
-0.5
-2
-1.5
-1
-0.5
0
0.5
1
1.5

Figure 2. Cyclic voltammograms of TiO_2 NTAs electrodes recorded at 20 mV s^{-1} in solutions of (a) 0.02 M $CuSO_4$ + 0.2 M $Na_3C_6H_5O_7$, (b) 0.01 M $SnCl_2$ + 0.2 M $Na_3C_6H_5O_7$ and (c) 0.2 M $ZnSO_4$ + 0.2 M $Na_3C_6H_5O_7$, 0.2 M $ZnSO_4$ + 0.2 M $Na_3C_6H_5O_7$ in 0.1 M or 3 M EDTA and (d) 0.02 M $CuSO_4$, 0.01 M $SnCl_2$ and 0.2 M $ZnSO_4$.

According to these findings, the UPD potentials of Cu and Sn (−0.500 and −0.120 V, respectively) lie within a roughly common UPD region (Figure 2-d), and the pH values of their precursor solutions are similar (6.30 and 6.88 respectively). This indicates that both elements can be simultaneously deposited on the substrate using the same potential. Figure 2c illustrates the CV of Zn onto TiO_2 NTAs substrate from a solution contains 0.20 M $ZnSO_4$ + 0.20 M trisodium citrate (pH = 5.3). The UPD reduction peak was identified at a potential of 0.210 V and bulk potential of −0.499 V (* in Figure 2c). The deposition of Zn should be in the UPD potential range of (−0.031 to 0.500 V) to prevent bulk deposition. However, the UPD potential for Zn was not lying in a common region with Cu and Sn and was more positive (black arrow in Figure 2d). Therefore, the UPD potential of Zn should be shifted to an appropriate common potential range within the UPD ranges of Cu and Sn to facilitate the simultaneous deposition of these elements and to prevent any bulk deposition of Zn when the common potential is applied.

Complexing agents can bring a stoichiometric deposition onto the substrate using UPD [24, 29], EDTA was used as a complexing agent in Zn precursor solutions to shift the UPD potential towards the negative (cathodic) side. Figure 2c illustrates the CVs of Zn on TiO_2 NTAs substrate before (0.00 M) and after adding EDTA (0.01 and 0.30 M) in Zn solutions. In this work, EDTA played a vital role in maintaining Zn complex to prevent Zn precipitation at more positive potentials. Zhang et al. have deposited CZTS on Ag substrate via EC-ALD [24]. They evidently demonstrated that adding 5 mM of EDTA to Cu solution maintained Cu complexes to avoid bulk deposition of Cu particles. In this study, UPD values in the range of -0.2 to -1 V were investigated to demonstrate the most effective deposition potential to synthesise the coaxial heterogeneous structure of the composite CZTS/TiO_2 NTAs. The UPD values to deposit CZTS onto TiO_2 NTAs should be correctly selected in order to ensure the simultaneous UPD of Cu, Zn and Sn on TiO_2 NTAs electrodes.

3.2 Crystalline phase and composition measurements

Figure 3 shows the XRD diffraction patterns of the pure and CZTS sensitised TiO_2 NTAs. The diffraction peaks located at 2θ = 25.4°, 37.9°, 48.0°, and 55.0°, corresponding to the crystalline orientations (101), (004), (200) and (211), respectively representing the anatase TiO_2 NTAs (Figure 3a). The peaks corresponding to the diffraction angles 2θ = 27.5°, 29.1°and 47.1° in Figure 3b represents the crystalline orientations of (101), (112) and (200) and

characterize the Kesterite structure of CZTS (ICDD No: 00-026-0575). Significantly, only the single-phase CZTS peaks, without any superfluous elements of Cu, Zn, Sn, and S, were identified.

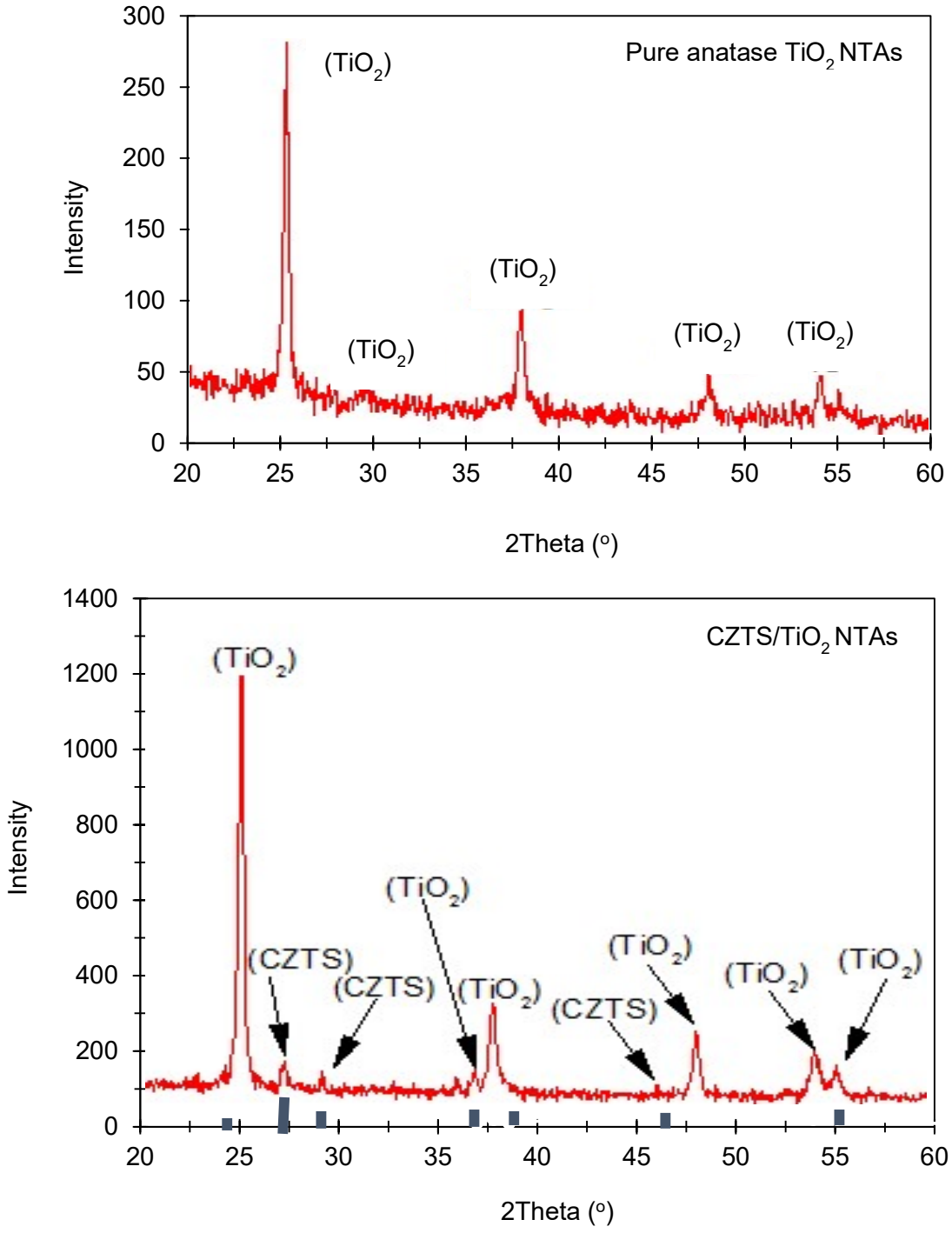

Figure 3. XRD diffractograms of XRD diffractograms of (a) pure anatase TiO_2 NTAs substrate annealed at 450.0 ℃ for 2 h and (b) CZTS electrodeposited onto TiO_2 NTAs at UPD potential = -0.500 V. Blue lines represents standard kesterite peaks.

Figure 4 shows the top-surface and cross section FEG-SEM images of pure TiO_2 NTAs. The structure of as-prepared CZTS/TiO_2 NTAs was determined *via* the top surface FEG-SEM image and EDX analysis (Figure 4). The well-organised pure TiO_2 NTAs were synthesised successfully *via* a two steps electrochemical anodization route. The inner diameter of the tube was estimated as ca. 111 ± 15 nm with a wall thickness of few nanometres (Figure 4). The FEG-SEM images show that the average inner diameter of the coated TiO_2 NTAs with CZTS reduced to ca. 100 nm, and the wall thickness became thicker relative to that in pure TiO_2 NTAs, suggesting that the coating layer was ca. 5.0 ± 0.5 nm. Furthermore, the well-ordered structure of the nanotubes was maintained after the electrodeposition of the elements. The cross section FEG-SEM image of pure TiO_2 NTAs exhibits that their length was approx. 220 ± 50 nm. The EDX spectrum illustrates that Cu, Zn, Sn and S were deposited on the surface of the TiO_2 NTAs.

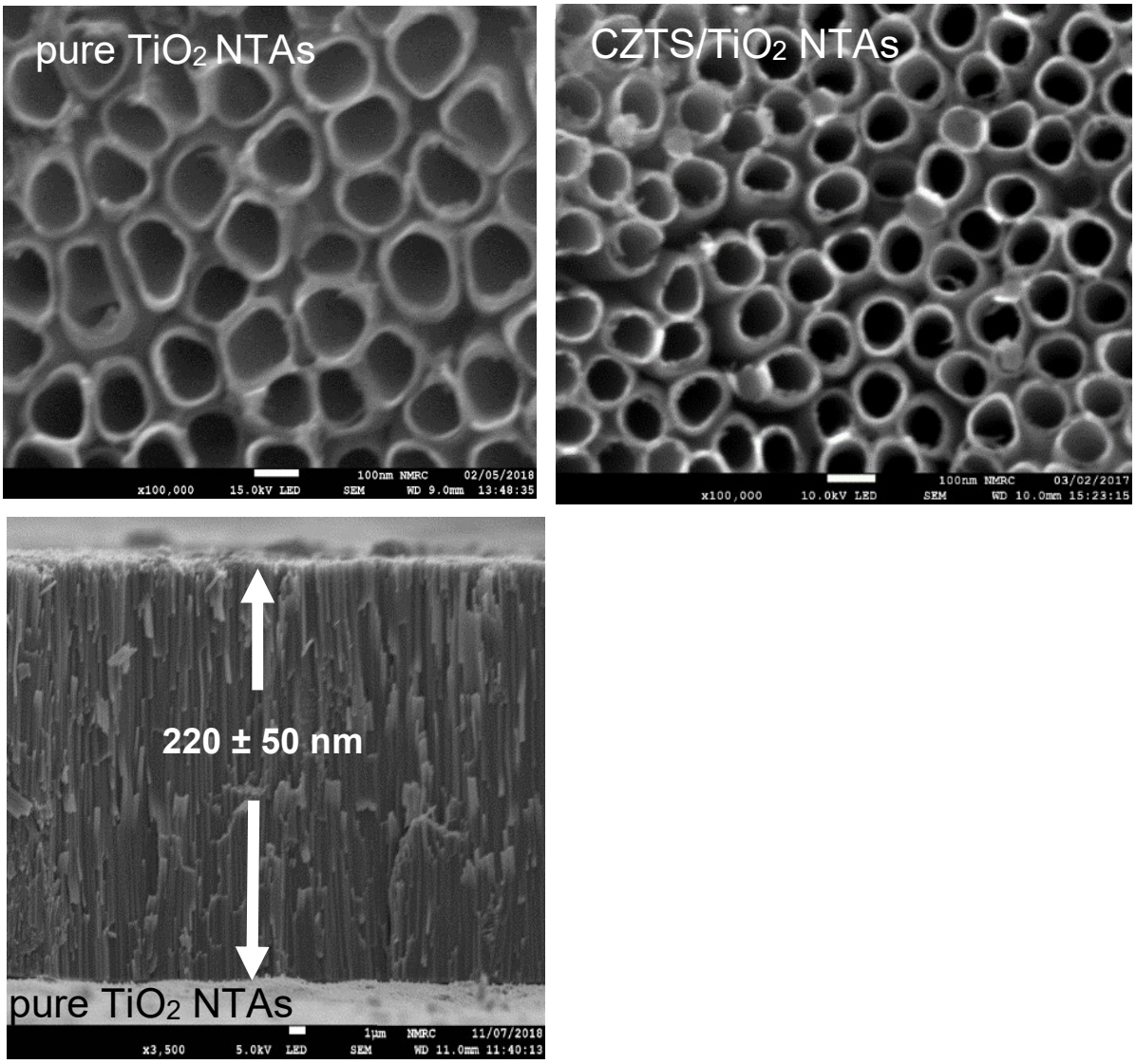

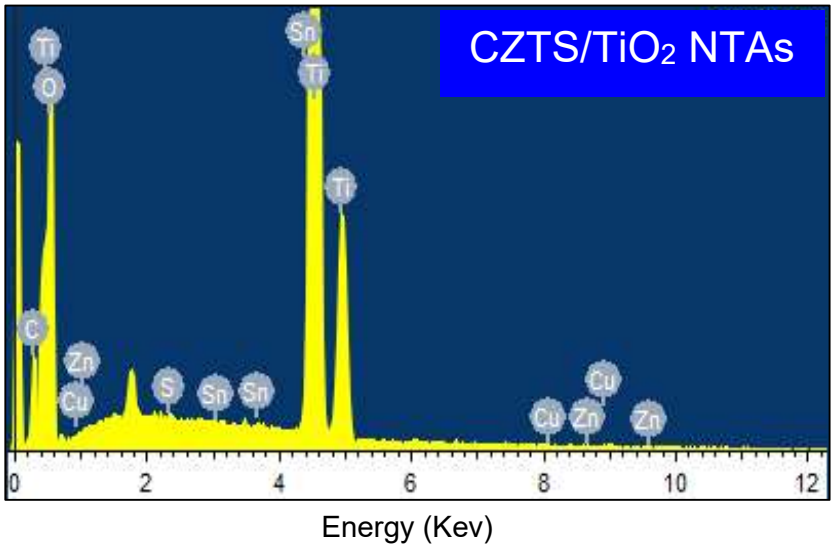

Figure 4. Top-surface (X100,000) and cross section (X3,500) FEG-SEM images of pure TiO_2 NTAs. Top surface FEG-SEM image (X100,000) and EDX analysis of CZTS electrodeposited onto TiO_2 NTAs electrodeposited on UPD potential = -0.500 V vs Ag/AgCl.

Figure 5 demonstrates the typical current density versus time relation during the simultaneous deposition of CZTS thin film *via* EC-ALD on TiO_2 NTAs at UPD potential of -0.5 V from a mix of precursor solutions of Cu, Zn, and Sn.

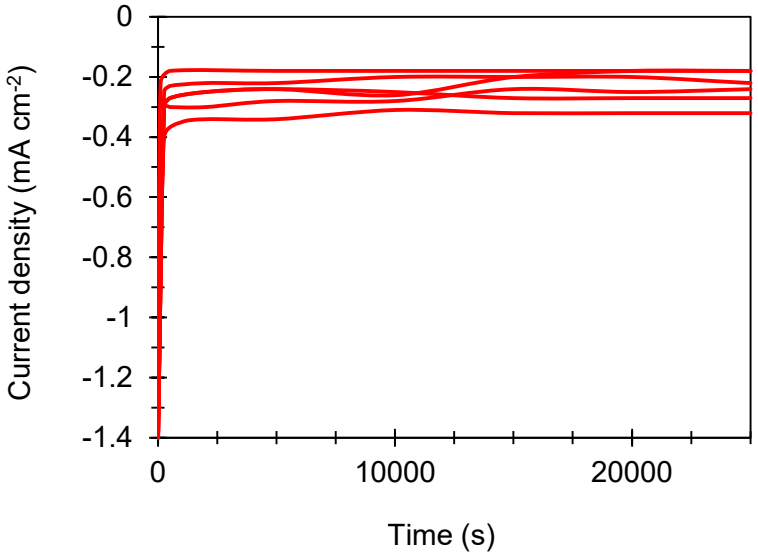

Figure 5. Current density versus time during the simultaneous deposition of CZTS thin films by EC-ALD on TiO_2 NTAs substrate at UPD potential = -0.500 V. Multiple scans represent the repeatability of the recoded current density for multiple EC-ALD.

Throughout the electrodeposition, the recorded cathodic current density exhibited almost a constant value ranging from -0.2 to -3.5 mA cm^{-2} for 25200 s, indicating that the well-organised structure of TiO_2 NTAs remained orderly and was not affected by the deposited

materials, owing to the absence of the bulk deposition of the metals. This finding was broadly repeated for the simultaneous deposition of CZT onto TiO_2 NTAs by using the EC-ALD route, which was shown by the multi scan of the recorded current density. Farinella et al. fabricated CZTS by a potentiostatic deposition from aqueous baths onto ITO substrates supported by polyethylene terephthalate (PET) [50]. They obtained CZTS in a bath of 2.5 ml of $CuSO_4$, 15 ml of $ZnSO_4$, 2.5 ml of $SnSO_4$ and 60 ml of $Na_2S_2O_3$ mixture, and the cathodic current density gradually reached a constant value of ~ -0.2 mA cm^{-2} after 1800 s.

UV-Vis measurements were performed to examine the capacity for harvesting the light from pure TiO_2 NTAs and CZTS/TiO_2 NTAs. Figure 6a illustrates the UV-Vis absorbance of pure TiO_2 NTAs and CZTS/TiO_2 NTAs.

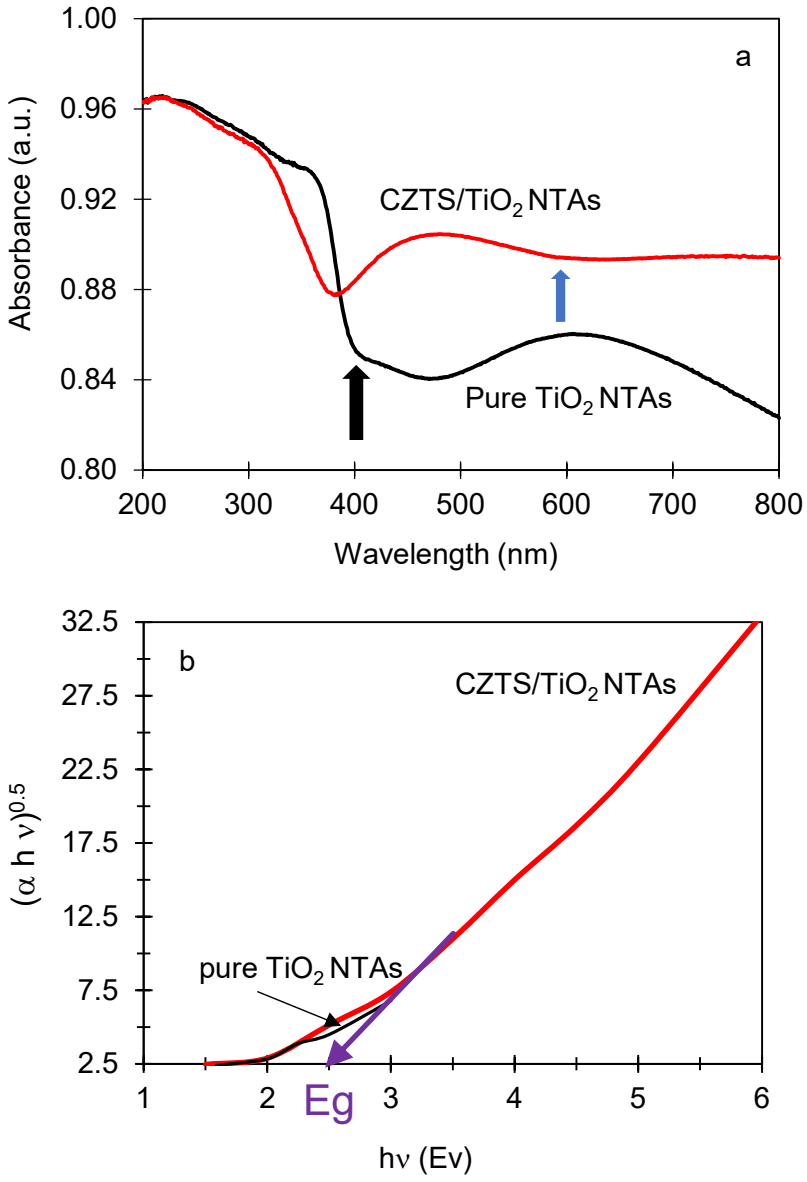

Figure 6 (a) UV-Vis absorbance spectra of pure TiO_2-NTAs and the as-synthesised CZTS/TiO_2 NTAs at UPD = -0.500 V, (b) Data of Figure 6a was transformed using the Kubelka−Munk function for the extraction of the optical bandgap energy (Eg) (purple arrow).

In comparison, with pure TiO_2 NTAs (400 nm), a significant shift in the wavelength towards the visible region (600 nm) for CZTS/TiO_2 NTAs was observed (red curve) (Figure 6a). The absorbance is determined by the absorption edge to determine its bandgap. The pure NTAs has an absorption edge in 400 nm (indicated by black arrow in the image). CZTS deposited NTAs has two absorption edge, one is around 400 nm, which derived from TiO_2 substrate, another has a redshifted absorption edge in the visible region and extends the absorption tail to 600 nm corresponding to the typical narrow band-gap semiconductor of CZTS (indicated by blue arrow in the image). After CZTS coating, the absorbance of the cascade structured CZTS/TiO_2 NTAs is apparently stronger than that of the pure TiO_2 NTAs in the visible region from 400 to 800 nm. The enhanced absorbance is believed to be caused by the CZTS coating layer, indicating that CZTS can promote the photo response, owing to its narrow bad-gap and capability of trapping holes. The bandgap energy was calculated from the relationship between the absorbance ($\propto$) and the incident photon energy ($h\nu$) (Figure 6b). The bandgap of pure TiO_2 NTAs was narrowed down from 3.10 eV to 2.43 eV after depositing CZTS on TiO_2 NTAs (Figure 6b).

Figure 7a shows the photocurrent density of the heterogeneous CZTS/TiO_2 NTAs that fabricated at deposition potential = -0.5 V; data for the corresponding pure TiO_2 NTAs before sensitisation is also provided. Figure 7b exhibits the photoconversion efficiency, which is defined as the overall ratio of the maximum energy output that can be obtained from the final products, hydrogen and oxygen to the energy supplied in the form of light to produce them [33]. The transient photocurrent curves to verify the light response of the pure and as-synthesised TiO_2 NTAs photoanodes were provided. Samples were exposed to pulsed illumination for 20 min (Figure 7c). The light was pulsed 1 min (on/off illumination) at an applied bias of 0.500 V vs. Ag/AgCl. The photocurrent density (1.8 mA cm^{-2}) of the samples that were deposited with CZTS was more than 3 times higher in comparison with the pure TiO_2 NTAs, (0.5 mA cm^{-2}). This variation in the photocurrent proves the improvement in the electrical conjunction leads to an enhancement in the light absorption ability of TiO_2 NTAs photoanode. This result can be attributed to the excellent deposition and the well-ordered CZTS/TiO_2 NTA structures. The photocurrent density reported in this study is higher than the values reported in the literature (0.1-1.75 mA cm^{-2}) for TiO_2 NTAs and composites such as bismuth oxyhalide [34, 52] and Bi_2MoO_6 [35] on TiO_2 NTAs [34-37, 51, 52].

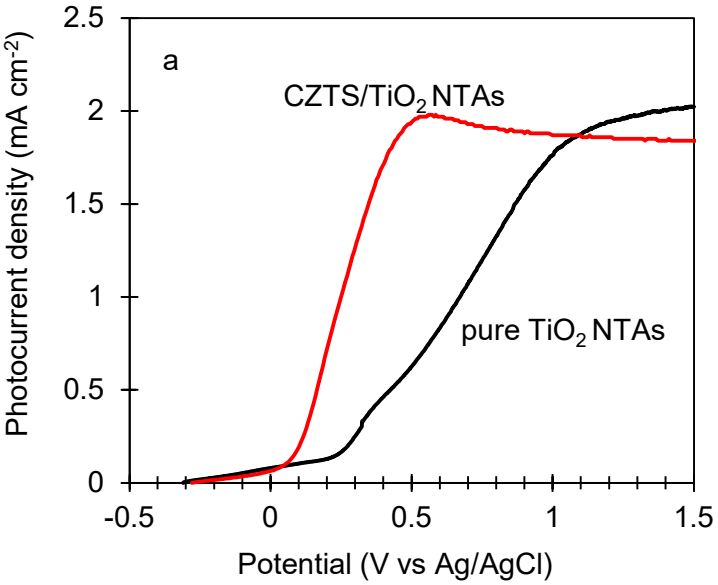
a
CZTS/TiO2 NTAs
pure TiO2 NTAs
Photocurrent density (mA cm-2)
Potential (V vs Ag/AgCl)
2.5
2
1.5
1
0.5
0
-0.5
0
0.5
1
1.5

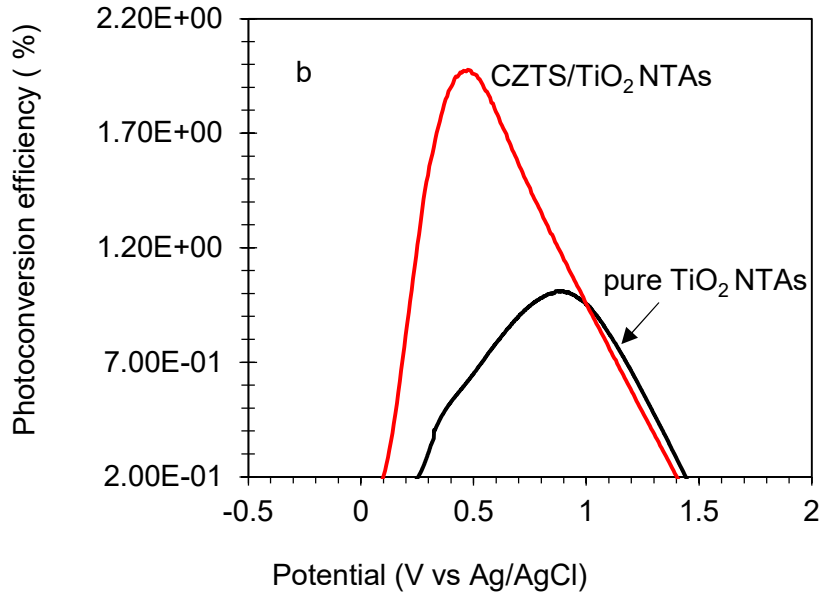
b
CZTS/TiO2 NTAs
pure TiO2 NTAs
Photoconversion efficiency (%)
Potential (V vs Ag/AgCl)
2.20E+00
1.70E+00
1.20E+00
7.00E-01
2.00E-01
-0.5
0
0.5
1
1.5
2

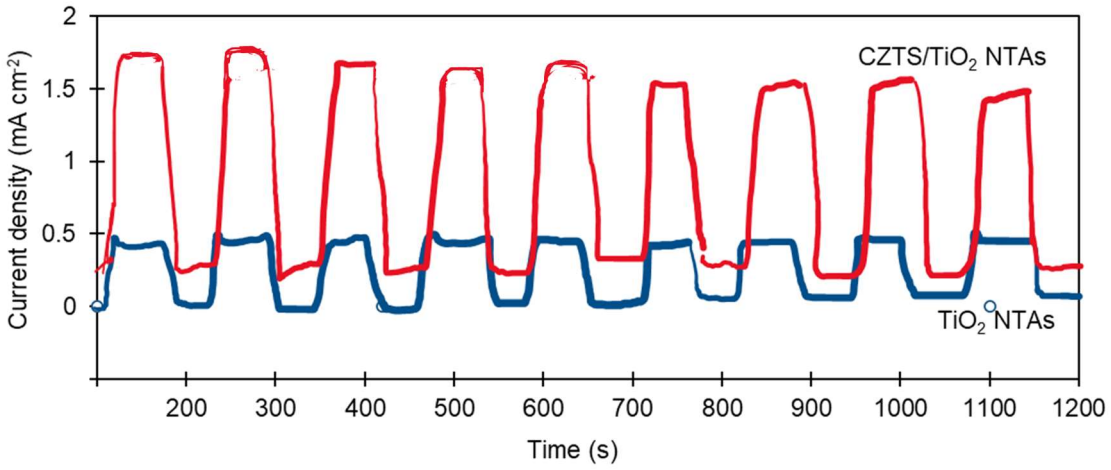
CZTS/TiO2 NTAs
TiO2 NTAs
Current density (mA cm-2)
Time (s)
2
1.5
1
0.5
0
200
300
400
500
600
700
800
900
1000
1100
1200

Figure 7 (a) Photocurrent density, (b) photoconversion efficiency and (c) photocurrent response of pulse illumination of pure TiO_2 NTAs and the as-synthesized CZTS/TiO_2 NTAs.

The as-synthesised CZTS/TiO_2 NTAs photoanode demonstrated an enhancement in the photoconversion efficiency to 2% in comparison with the pure TiO_2 NTAs (1.1%). A maximum hydrogen generation rate of 49 ml h^{-1} cm^{-2} from CZTS/TiO_2 NTAs photo-electrode was achieved under light irradiation. This rate is much higher than the range of 0.41 to 14.2 ml h^{-1} cm^{-2} that was reported in the literature for the water-splitting applications (Table 1) [32, 33, 37-39, 53-54].

Table 1. Comparison of hydrogen production rate of this study with literature.

Material	H_2 production rate (ml h^{-1} $cm^{-2)}$	Reference
CZTS/TiO_2 NTAs	49	This work
Pt-N doped/TiO_2	8.4	[53]
Bi/Bi_2MoO_6/TiO_2 NTAs	1.76	[32]
Bi_2S_3-BiOBr/TiO_2 NTAs	0.41	[33]
Ag/Fe/TiO_2 NTAs	0.0341	[39]
TiO_2 NTAs	1.3	[54]

4. Conclusion

This study presented and discussed a successful simultaneous underpotential deposition of multiple elements onto TiO_2 NTAs substrates using the EC-ALD technique from mixed precursor solutions for the first time. The Kesterite structure of CZTS was successfully synthesised as a single phase without superfluous elements of Cu, Zn, Sn, and S. A red shift was observed from 400 nm for pure nanotubes to 600 nm for CZTS/TiO_2 NTAs, respectively. The bandgap was narrowed from 3.1 eV of pure TiO_2 NTAs to 2.43 eV of CZTS/TiO_2 NTAs. After sensitising the nanotubes with CZTS, an enhancement in the photoconversion efficiency (from 1.1% to 2%) was obtained. More importantly, the well-organised nanotube morphology was maintained after the coating with CZTS using the EC-ALD technique without clogging the tube mouths. The thickness of CZTS layer was estimated ca. 5.0 ± 0.5 nm and the average inner diameter of TiO_2 NTAs was reduced from ca. 111 ± 15 nm (pure TiO_2 NTAs) to ca. 100 nm after the sensitisation with the CZTS thin film. The novel photoanode of CZTS/TiO_2 NTAs demonstrated a synergistic effect on the photocatalytic properties and the hydrogen generation rate of 49 ml h^{-1} cm^{-2}.

Acknowledgements

The authors would like to thank the Higher Committee for Education Development in Iraq for a studentship to A. Al-Shihabi Al-Ani, and Ningbo Municipal Government for financial

support to G. Z. Chen (3315 Plan and 2014A35001-1). Dr J. A. Fernands is gratefully acknowledged for his assistance in UV-Vis measurements in the GSK Carbon Neutral Laboratory for Sustainable Chemistry at the University of Nottingham. The authors also thank the Nanoscale and Microscale Centre (nmRC) for providing access to characterisation instruments.

References

1. Fujishima, A. and K. Honda, Electrochemical Photolysis of Water at a Semiconductor Electrode. Nature, 1972. 238: p. 37.
2. Li, X., et al., Engineering heterogeneous semiconductors for solar water splitting. Journal of Materials Chemistry A, 2015. 3(6): p. 2485-2534.
3. Raja, K.S., V.K. Mahajan, and M. Misra, Determination of photo conversion efficiency of nanotubular titanium oxide photo-electrochemical cell for solar hydrogen generation. Journal of Power Sources, 2006. 159(2): p. 1258-1265.
4. Nowotny, J., et al., Solar-hydrogen: Unresolved problems in solid-state science. Solar Energy, 2005. 78(5): p. 593-602.
5. Park, J.H., S. Kim, and A.J. Bard, Novel carbon-doped TiO_2 nanotube arrays with high aspect ratios for efficient solar water splitting. Nano letters, 2006. 6(1): p. 24-28.
6. Grimes, C.A. and G.K. Mor, TiO_2 nanotube arrays: synthesis, properties, and applications. 2009: Springer Science & Business Media.
7. Mor, G.K., et al., Vertically oriented Ti− Fe− O nanotube array films: toward a useful material architecture for solar spectrum water photoelectrolysis. Nano letters, 2007. 7(8): p. 2356-2364.
8. Macak, J.M., et al., Self-Organized TiO_2 Nanotube Layers as Highly Efficient Photocatalysts. small, 2007. 3(2): p. 300-304.
9. Mor, G.K., et al., Use of highly-ordered TiO_2 nanotube arrays in dye-sensitized solar cells. Nano letters, 2006. 6(2): p. 215-218.
10. Wang, H., et al., Improvement of photocatalytic hydrogen generation from CdSe/CdS/TiO_2 nanotube-array coaxial heterogeneous structure. International Journal of Hydrogen Energy, 2014. 39(1): p. 90-99.
11. Khaselev, O. and J.A. Turner, A Monolithic Photovoltaic-Photoelectrochemical Device for Hydrogen Production via Water Splitting. Science, 1998. 280(5362): p. 425-427.
12. Khan, S.U.M., M. Al-Shahry, and W.B. Ingler, Efficient Photochemical Water Splitting by a Chemically Modified n-TiO_2. Science, 2002. 297(5590): p. 2243-2245.
13. Mor, G.K., et al., p-Type Cu− Ti− O nanotube arrays and their use in self-biased heterojunction photoelectrochemical diodes for hydrogen generation. Nano Letters, 2008. 8(7): p. 1906-1911.
14. Feng, X., et al., Vertically aligned single crystal TiO_2 nanowire arrays grown directly on transparent conducting oxide coated glass: synthesis details and applications. Nano letters, 2008. 8(11): p. 3781-3786.
15. Kim, D., et al., Bamboo-type TiO_2 nanotubes: improved conversion efficiency in dye-sensitized solar cells. Journal of the American Chemical Society, 2008. 130(49): p. 16454-16455.
16. Mohapatra, S.K., et al., Functionalization of self-organized TiO2 nanotubes with Pd nanoparticles for photocatalytic decomposition of dyes under solar light illumination. Langmuir, 2008. 24(19): p. 11276-11281.
17. Ge, M., et al., One-dimensional TiO_2 Nanotube Photocatalysts for Solar Water Splitting. Advanced Science, 2017. 4(1).
18. Katagiri, H., et al., Enhanced conversion efficiencies of Cu_2ZnSnS_4-based thin film solar cells by using preferential etching technique. Applied physics express, 2008. 1(4): p. 041201.

19. Ito, K. and T. Nakazawa, Electrical and optical properties of stannite-type quaternary semiconductor thin films. Japanese Journal of Applied Physics, 1988. 27(11R): p. 2094.
20. Lin, Y.-P., et al., Preparation of Cu_2ZnSnS_4 (CZTS) sputtering target and its application to the fabrication of CZTS thin-film solar cells. Journal of Alloys and Compounds, 2016. 654: p. 498-508.
21. Zhou, W., et al., 2012. Study on the effects of 5d energy locations of Ce^{3+} ions on NIR quantum cutting process in Y_2SiO_5: Ce^{+}, Yb^{3+}. Optics express, 20**,** A510-A518.
22. Wang, W., et al, 2014c. Device characteristics of CZTSSe thin-film solar cells with 12.6% efficiency. Advanced Energy Materials, 4**,** 1301465.
23. Nguyen, D.-C., et al., 2015. Effects of annealing conditions on crystallization of the CZTS absorber and photovoltaic properties of Cu(Zn, Sn)(S, Se)$_2$ solar cells. Journal of Alloys and Compounds, 632**,** 676-680
24. Wang, Z. & Demopoulos, G. P. 2015. Growth of Cu_2ZnSnS_4 nanocrystallites on TiO_2 nanorod arrays as novel extremely thin absorber solar cell structure via the successive-ion-layer-adsorption-reaction method. ACS applied materials & interfaces, 7**,** 22888-22897.
25. Lin, Y.-P., et al.,2016b. Preparation of Cu_2ZnSnS_4 (CZTS) sputtering targe t and its application to the fabrication of CZTS thin-film solar cells. Journal of Alloys and Compounds, 654**,** 498-508.
26. Gan, T., et al., Cu2ZnSnS4@TiO2 p-n heterostructured nanosheet arrays: Controllable hydrothermal synthesis and enhanced visible light-driven photocatalytic activity. Applied Surface Science, 2017. 408: p. 60-67.
27. Wang, Z., Nanoengineering of the Cu_2ZnSnS_4–TiO_2 interface *via* atomic layer deposition of Al_2O_3 for high sensitivity photodetectors and solid state solar cells. J. Mater. Chem. A., 2018. 6: p. 11507-11520.
28. Bogatu, C., et al., Stability of the Cu2ZnSnS4/TiO2 photocatalytic thin films active under visible light irradiation. Catalysis Today, 2019. 328: p. 79-84.
29. Saleem, M.R., et al., Impact of atomic layer deposition to nanophotonic structures and devices. Frontiers in Materials, 2014. 1: p. 18.
30. Scragg, J.J., Studies of Cu_2ZnSnS_4 films prepared by sulfurisation of electrodeposited precursors. 2010, University of Bath.
31. Ghosh, S., et al., 2000. Deposition of thin films of different oxides of copper by RF reactive sputtering and their characterization. Vacuum, 57**,** 377-385
32. Cao, D., et al, Solvothermal synthesis and enhanced photocatalytic hydrogen production of Bi/Bi2MoO6 co-sensitized TiO2 nanotube arrays. Separation and Purification Technology, 2020. 250: p.117132.
33. Jia, Y., et al., Construction of Bi2S3-BiOBr nanosheets on TiO2 NTA as the effective photocatalysts: Pollutant removal, photoelectric conversion and hydrogen generation. Journal of Colloid and Interface Science, 2021. 585: p. 459-469.
34. Liu, Z. et al., Vertical grown BiOI nanosheets on TiO2 NTs/Ti meshes toward enhanced photocatalytic performances. Journal of Alloys and Compounds, 2020. 820: p. 153109.
35. Liu, Z. et al., Solvothermal fabrication and construction of highly photoelectrocatalytic TiO2 NTs/Bi2MoO6 heterojunction based on titanium mesh. Journal of Colloid and Interface Science, 2019. 556: p. 92-101.
36. Wang, Q, et al., Morphology regulated Bi2WO6 nanoparticles on TiO2 nanotubes by solvothermal Sb3+ doping as effective photocatalysts for wastewater treatment. Electrochimica Acta, 2020. 330: p. 135167.
37. Li, Y., et al., Effect of water and annealing temperature of anodized TiO_2 nanotubes on hydrogen production in photoelectrochemical cell. Electrochimica Acta*,* 2013b. 107: p. 313-319.
38. Li, G., et al., Highly Active Photocatalyst of Cu_2O/TiO_2 Octahedron for Hydrogen Generation. ACS Omega, 2019. 4: p. 3392–3397.

39. Fan, X., et al., Preparation and characterization of Ag deposited and Fe doped TiO2 nanotube arrays for photocatalytic hydrogen production by water splitting. Ceramics International, 2014. 40: p. 15907-15917.

40. Hou, X., et al., Highly efficient photocatalysis of p-type Cu_2ZnSnS_4 under visible-light illumination. Materials Research Bulletin, 2014. 60: p. 628-633.
41. Zhang, X., et al., Electrochemical deposition of quaternary Cu_2ZnSnS_4 thin films as potential solar cell material. Applied Physics A, 2009. 94(2): p. 381-386.
42. Reith, P. and G. Hopman, Investigating electrodeposition to grow CZTS thin films for solar cell applications. 2012, University of Twente.
43. Ho, T.-Y. and L.-Y. Chen, The Study of Cu2ZnSnS4 Nanocrystal/TiO_2 Nanorod Heterojuction Photoelectrochemical Cell for Hydrogen Generation. Energy Procedia, 2014. 61: p. 2050-2053.
44. Chi, C.-F., et al., Energy level alignment, electron injection, and charge recombination characteristics in CdS/CdSe cosensitized TiO_2 photoelectrode. Applied Physics Letters, 2011. 98(1): p. 012101.
45. Niitsoo, O., et al., Chemical bath deposited CdS/CdSe-sensitized porous TiO_2 solar cells. Journal of Photochemistry and Photobiology A: Chemistry, 2006. 181(2): p. 306-313.
46. Zhu, W., et al., Coaxial Heterogeneous Structure of TiO_2 Nanotube Arrays with CdS as a Superthin Coating Synthesized via Modified Electrochemical Atomic Layer Deposition. Journal of the American Chemical Society, 2010. 132(36): p. 12619-12626.
47. Hassanien, A. and Akl, A. A., Effect of Se addition on optical and electrical properties of chalcogenide CdSSe thin films. Superlattices and Microstructures, 2016. 89**:** p. 153-169.
48. Ghrairi, N. and Bouaicha, M. 2012. Structural, morphological, and optical properties of TiO_2 thin films synthesized by the electro phoretic deposition technique. Nanoscale research letters, 2012. 7**:** p. 357.
49. Murphy, A., Band gap determination from diffuse reflectance measurements of semiconductor films, and application to photoelectrochemical water-splitting. Solar Energy Materials and Solar Cells, 2007. 91(14): p. 1326-1337.
33.
34. .
35.
50. Farinella, M., et al., Electrochemical deposition of CZTS thin films on flexible substrate. Energy Procedia, 2014. 44**:** p. 105-110.
51. Wang, Y., CTAB-assisted solvothermal construction of hierarchical Bi2MoO6/Bi5O7Br with improved photocatalytic performances. Separation and Purification Technology, 2020. 242: p. 116775.
52. Liu, Z. et al., Enhanced photocatalytic performance of TiO2 NTs decorated with chrysanthemum-like BiOI nanoflowers. Separation and Purification Technology, 2019. 215: p. 565-572.
53. Setiadi, S. A., Photocatalytic hydrogen generation from glycerol and water using Pt loaded N-doped TiO_2 nanotube., International Journal of Engineering Technology, 2011. 11(3): p. 91-95.
54. Smith, Y.R., et al., Single-step anodization for synthesis of hierarchical TiO2 nanotube arrays on foil and wire substrate for enhanced photoelectrochemical water splitting, International Journal of Hydrogen Energy, 2013. 38: p. 2062-2069.

55. Ye, M., et al., High-efficiency photoelectrocatalytic hydrogen generation enabled by palladium quantum dots-sensitized TiO_2 nanotube arrays. Journal of the American Chemical Society, 2012. 134: p. 15720-15723.